electronics

MDPI

Article

The Influence of Different Levels of Cognitive Engagement on the Seated Postural Sway

Daniele Bibbo *, Silvia Conforto, Maurizio Schmid and Federica Battisti

Department of Engineering, University of Roma Tre, Via Vito Volterra, 62, 00146 Rome, Italy; silvia.conforto@uniroma3.it (S.C.); maurizio.schmid@uniroma3.it (M.S.); federica.battisti@uniroma3.it (F.B.)

* Correspondence: daniele.bibbo@uniroma3.it; Tel.: +39-06-5733-7298

Received: 5 March 2020; Accepted: 30 March 2020; Published: 31 March 2020

Abstract: In this paper, we introduced and tested a new system based on a sensorized seat, to evaluate the sitting dynamics and sway alterations caused by different cognitive engagement conditions. An office chair was equipped with load cells, and a digital and software interface was developed to extract the Center of Pressure (COP). A population of volunteers was recruited to evaluate alterations to their seated posture when undergoing a test specifically designed to increase the cognitive engagement and the level of stress. Relevant parameters of postural sway were extracted from the COP data, and significant alterations were found in all of them, highlighting the ability of the system to capture the emergence of a different dynamic behavior in postural control when increasing the complexity of the cognitive engagement. The presented system can thus be used as a valid and reliable instrument to monitor the postural patterns of subjects involved in tasks performed in a seated posture, and this may prove useful for a variety of applications, including those associated with improving the quality of working conditions.

Keywords: seated posture; cognitive engagement; stress level; load cells; embedded systems; sensorized seat

1. Introduction

Modern lifestyle is more and more characterized by the fact that people are moving less and are spending an increasing amount of time sitting [1–4]. This takes into account the time spent working in front of a PC or using means of transportation to move from one place to another. Many leisure activities are also performed while seated (e.g., reading a book, watching television).

A sedentary lifestyle is dangerous for many reasons. It may lead to the development of chronic diseases (e.g., cardiovascular) [5,6] and may also affect psychological health [7]. Another problem related to the increase of time spent sitting is that the position adopted on the chair is often incorrect, thus creating health problems such as back pain [6] and headaches [7].

In recent years, people have become more aware of these problems. This is witnessed by the commercialization of height-adjustable sit–stand desks, but also by the spread of many low-cost devices such as smart watches (e.g., Fitbit trackers, Apple watches) and applications (e.g., Stand Up! The Work Break Timer, Time Out) that push the users to perform micro-breaks every 20–30 min of continuous sitting. In this regard, Sitting Posture Monitoring Systems (SPMS) have been introduced in the community, with the objective of detecting and understanding the position of a person in the seated position.

SPMS can rely on different technologies, which span from the use of wearable sensors [8–13], to the use of cameras [14–16], and also to the use of optoelectronic systems [17]. In all the considered cases, the aim is to provide the user with a minimally intrusive experience, so that the SPMS does not interfere with the normal behavior.

Among the available solutions, a state-of-the-art solution is that of equipping chairs with sensors able to collect data on the posture of the user [18–21]: Ishac et al. in [18] presented a cushion to be used in the backrest of the chair. The cushion is equipped with a pressure sensing array that allows the measurement of the pressure at 9 different points. The lack of information about the pressure on the seat reduces the amount of information that can be extracted.

Zemp et al. in [19] used an innovative approach based on machine learning to classify the data collected by 16 pressure sensors located on different parts of a chair (armrest, seat and backrest). While allowing an improved posture classification, the computational complexity of this algorithm is quite high.

Similarly, Roh et al. in [20] inserted load cells in the frame of the chair to record data that are processed through a machine learning approach. In this work, even if a dynamic evaluation of the sitting posture is achieved, data are used only to classify postures and not to evaluate the dynamic behavior of a subject in different conditions.

In a previous work [21], we equipped an office chair with textile sensors that allowed us to recognize 8 different sitting positions. We experimented a limitation since the smart chair allows only the detection of specific positions and not to monitor their evolution in time.

To evaluate the dynamic features of the seated position, we took inspiration from the use of force plates in posturography: in that domain, a three-component force plate is generally used to record over time where the Center of Pressure (COP) is located, by measuring and combining the vertical force component and the two torque components applied on it [22]. The COP is defined as the application point of the ground reaction force, and, in upright stance, it sways dynamically around an equilibrium point even in absence of external disturbances [23], a phenomenon that is generally denoted as postural sway. Postural sway is controlled by the Central Nervous System (CNS) in an autonomous way, and it is strictly related to the human capability of standing [24]. Human standing position is influenced by many disturbing factors (external, such as audio or visual stimuli, or internal, such as respiration or cardiac activity [25,26]) that are continuously compensated by the CNS.

Similarly, while seated, the human body is subject to a number of disturbances and, also in this condition, the CNS modulates the activity of muscles to maintain the equilibrium of the upper body segments (e.g., upper trunk, head, upper limbs) [27]. Correspondingly, in a seated position it is possible to determine where the Upper body Center of Pressure (UCOP) is located over a period of time, in order to evaluate, for example, if, in the presence of different external stimuli, or during task execution, a different way of swinging can be identified and to what it can be associated.

In both cases the equilibrium can be affected by different cognitive load levels of the task that a subject is performing. Different levels of cognitive load can be associated with variations of the electroencephalogram (EEG) signal [28]. In [29] the authors show that the EEG signal can be used to monitor different levels of stress. Moreover, it is known that an increase of cognitive load induces increasing levels of stress [30].

Among the techniques used to increase the cognitive load, the analysis of the EEG signals has proven that the Stroop Test activates brain areas related to attention [31]. Since this test can be a valuable tool to induce different cognitive loads on subjects, it has been used in the experiments presented in this work and it will be detailed in the following.

Anyway, EEG-based techniques require complex setup to record this type of signals. For this reason, EEG is not the most convenient means to monitor the level of stress in common daily life activities, such as in workplaces. Among the possible alternatives, it has been demonstrated that both eye movements and postural sway can be associated to different levels of cognitive involvement: in [32], 16 volunteers were asked to perform visual tasks while standing and they highlight the presence of a synergic relation between recorded eye and body movements for high precision tasks; moreover, even if some categories of trained people (e.g., activities that requires more equilibrium such as dancing) are in general more stable, everybody has a tendency to swing more when a demanding task is required [33], and this evidence makes space for the possibility to monitor cognitive load through

the variations in postural sway. Following along this line, in [34], a Nintendo Wii balance board was selected to analyze the postural sway of older adults with no cognitive disability while performing predefined tasks in a home environment. In this case also, postural sway has been correlated to the cognitive status of the examined subjects.

In this work, the seated postural sway was analyzed using an innovative instrumented chair able to collect in a non-invasive way the instantaneous position of the UCOP. To test its validity, we asked subjects to perform a task sequence with increasing levels of cognitive engagement. As demonstrated in [21], increasing levels of cognitive engagement modify the posture that, starting from a relaxed seated condition will reach a stressed one, but up to now this was not quantified by the amount of seated postural sway associated with the observed modifications in posture.

2. Materials and Methods

2.1. Instrumented Chair Design

To evaluate the seated postural sway, a new instrumented chair has been designed and realized starting from previous experiences [21,35,36], where pressure sensors have been used to determine static postures of the users. In this work, an office chair was equipped with a set of four force sensors placed under its Load Plane (LP, i.e., where the pelvis loads up the chair). This set up was used to extract the instantaneous position of the UCOP mediolateral and anteroposterior coordinates (i.e., X_{UCOP} and Y_{UCOP}), under the hypothesis that the remaining body segments (thighs, legs, foot) do not concur to loading the seat.

In analogy to posturography in an upright stance, the required dynamic components to calculate the UCOP coordinates are: the resultant vertical force applied on LP F_z, that is the force component acting along the perpendicular Z axis; and the two torques M_x and M_y applied around the orthogonal axes identified on the load plane, identified as X and Y (Figure 1).

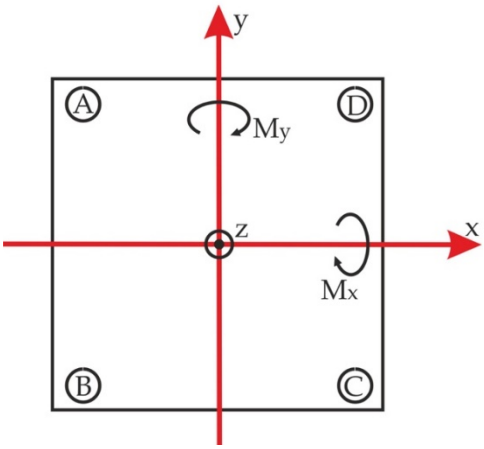

Figure 1. Scheme of the instrumented chair load plane: The reference system for the dynamic components are identified by (x,y,z) axes, while the load cells positions are identified by the {A,B,C,D} markers.

Considering that M_x and M_y are defined as the vector product of F_z and the distance of its point of application on LP from each axis, the values of the UCOP coordinates, X_{UCOP} and Y_{UCOP}, can be obtained as:

$$X_{UCOP} = \frac{M_y}{F_z}; \; Y_{UCOP} = -\frac{M_x}{F_z}. \quad (1)$$

To evaluate these three dynamic components, four load cells can be inserted in the positions {A,B,C,D} of the LP (Figure 1) and the four force components {F_A, F_B, F_C, F_D} can be measured. Consequently, F_z can be obtained as:

$$F_z = F_A + F_B + F_C + F_D. \tag{2}$$

Each load cell produces a voltage output V_P that in linear conditions results:

$$F_P = k_P V_P \tag{3}$$

where P = {A,B,C,D} represents the position and k_P is a proportionality constant.

If F_Z is applied in the center of the LP (i.e., $X_{UCOP} = 0$, $Y_{UCOP} = 0$) the four load cells are equally loaded and the torques applied around the X and Y axes are equal to zero, so it results:

$$k_A V_A = k_B V_B = k_C V_C = k_D V_D = 0.25 \times F_z. \tag{4}$$

Considering that four load cells with the same features are used (thus the proportionality constant is the same for all the load cells), the previous equation can be approximated by:

$$F_z = K_z(V_A + V_B + V_C + V_D) = K_z V_{Fz} \tag{5}$$

with K_Z the common constant of proportionality for the F_z measurement.

When F_Z is applied on a point that does not lie on one or both axes, one or both torque components are applied on the LP.

For example, when F_z is applied in a generic point on the x axis different from zero, a M_x component results on the LP; in this case the four load cells are loaded in a different way and it results that:

$$M_x = \frac{l}{2}[(k_B V_B + k_C V_C) - (k_A V_A + k_D V_D)] \tag{6}$$

where *l* is the distance between A and B (or between C and D).

This equation represents the sum of each torque contribution given by the force reactions, due to F_z solicitation, applied in the four P positions. Since the hypothesis of using load cells with the same features still holds, the previous equation can be approximated by:

$$M_x = \frac{lK_z}{2}[(V_B + V_C) - (V_A + V_D)] = K_x[(V_B + V_C) - (V_A + V_D)] = K_x V_{Mx} \tag{7}$$

with K_y a general constant of proportionality.

With similar considerations, it is possible to write that:

$$M_y = K_y[(V_C + V_D) - (V_A + V_B)] = K_y V_{My}. \tag{8}$$

It is then possible to measure F_z, M_X and M_y if the three parameters {K_x, K_y, K_z} and the four voltage values {V_A, V_B, V_C, V_D} are known. This computation allows to compute the UCOP coordinates, $X_{UCOP\ and}$ Y_{UCOP}.

Each force component can be measured by a load cell and, after the signals are acquired, the mechanical quantities values can be calculated combining the digitalized data. These equations are valid in ideal conditions, where the cross-talk effect among channels (i.e., the influence of a specific load on all output channels, given by multiple factors) is neglected. In real conditions, every mechanical quantity is obtained taking in account cross-talk effects and properly modifying the given equations with a corrective factor; this is usually achieved by a calibration procedure that will be described in the following.

Using a normal office chair, four commercial load cells were placed in the four corners of its seat, to realize an instrumented system, where an LP can be identified, with the features described above. A custom frame was realized and used to partially replace the chair frame to obtain four areas of where to place the load cells (Figure 2). The custom frame was designed in order not to flex during dynamic solicitation, and not to affect the measures performed with the load cells.

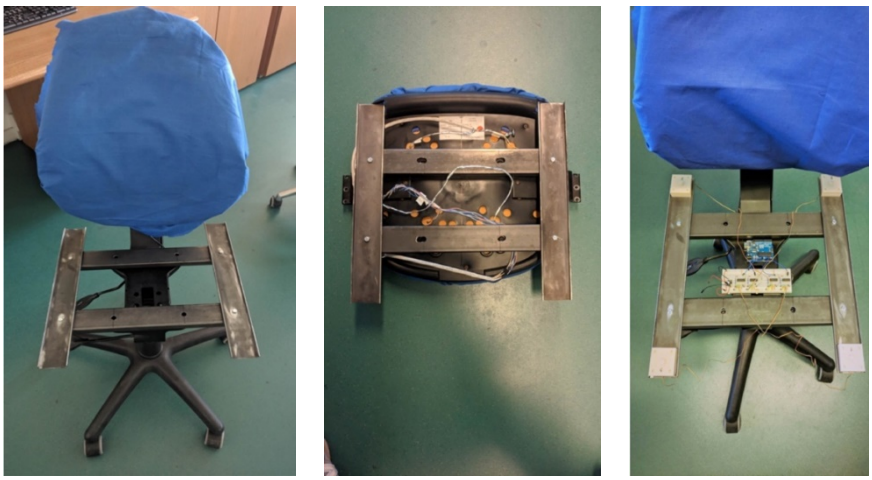

(**a**) (**b**) (**c**)

Figure 2. Custom frame realized to house the load cells: (**a**) first part of the new frame fixed on the chair structure; (**b**) second part of the new frame fixed under the seat; (**c**) load cells housing.

The load cells used in this project are the FX1901 class (Measurement Specialties Inc., TE Connectivity Group, USA), while the specific used model (FX1901-0001-0100-L) is a 1% load cell device with full scale ranges of 100lb compression (about 45kg). These devices, specifically designed for force sensing in "smart" consumer and medical products, use micro-machined piezoresistive strain gauges, showing a ratiometric span of 20 mV/V.

To place the load cells under the LP, a specific adaptor was designed and realized by means of a 3D printing process. A Stratasys Objet30 Prime was used: this machine allows polyJet 3D printing that allows the realization of high-resolution components by jetting microscopic layers of liquid photopolymer onto a build tray and instantly curing them with UV light. This accuracy in realization, comparable with a high accuracy machining of metal alloy, was necessary to couple the 4 load cells with the flat surface of the metal frame where they have been housed. In Figure 3, one of the realized adaptors is shown: the load cell is fixed to the lower part of the adaptor and is covered by a two-piece top part. This part presents a cylindrical element that is in contact with the load-sensitive part of the load cell and with the top part of the custom chair frame, thus transmitting directly to the load cell the force applied on the LP.

Each load cell, as mentioned above, was realized using strain gauges that are assembled in a full Wheatstone bridge configuration. As mentioned in its datasheet, a 4-wire connection is provided: 2 wires are used to supply the Wheatstone bridge $\{+V_{in}, -V_{in}\}$, while 2 wires are used to measure its outputs $\{+V_{out}, -V_{out}\}$.

The four load cells were driven independently using four instrumentation amplifiers, INA125 (Texas Instruments inc., USA). It is a high-accuracy instrumentation amplifier with a precision voltage reference used to provide a complete bridge excitation and that can receive and amplify differentially the bridge output. The gain was set using the dedicated single external resistor pin, using the datasheet information (selectable gain from 4 to 10,000) in order to best fit the voltage range of the adopted A/D converter. This last operation was performed using an Arduino Uno (Arduino cc) board, that through an ATmega328P microcontroller provided the necessary function to acquire

signals. A specific firmware was realized to acquire from four input channels of the Arduino board the four INA125 output analog signals with a 100 Hz sampling frequency.

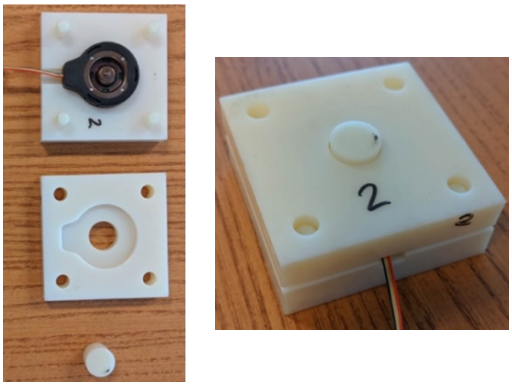

(**a**) (**b**)

Figure 3. Load cells housing adaptors: (**a**) open adaptors; (**b**) closed adaptor with enclosed load cell: the central cylindrical element is in contact with the load-sensitive part of the load cell.

The AD converter was managed by using a custom interface realized with Labview (National Instruments, USA) that allows the connection with the Arduino board via USB. The designed and realized Labview panel (i.e., Virtual Instrument, VI), allows the serial port connection to receive the digitalized data that are converted from bit levels to mechanical quantities using proper calibration coefficients. Moreover, the VI calculates in real time the UCOP coordinates and all data (i.e., F_z, M_x and M_y together with X_{UCOP} Y_{UCOP}) are saved in a file for further elaboration.

The mechanical quantities in real conditions, where cross-talk effects are present, are obtained from the acquired voltage values according to the following equations:

$$\begin{cases} F_z = a_{11}V_{Fz} + a_{12}V_{Mx} + a_{13}V_{My} \\ M_x = a_{21}V_{Fz} + a_{22}V_{Mx} + a_{23}V_{My} \\ M_y = a_{31}V_{Fz} + a_{32}V_{Mx} + a_{33}V_{My} \end{cases} \Rightarrow \begin{pmatrix} F_z \\ M_x \\ M_y \end{pmatrix} = \begin{pmatrix} a_{11} & a_{12} & a_{13} \\ a_{21} & a_{22} & a_{23} \\ a_{31} & a_{32} & a_{33} \end{pmatrix} \begin{pmatrix} V_{Fz} \\ V_{Mx} \\ V_{My} \end{pmatrix} \quad (9)$$

with $\begin{pmatrix} a_{11} \\ a_{22} \\ a_{33} \end{pmatrix} = \begin{pmatrix} K_z \\ K_x \\ K_y \end{pmatrix}$ and a_{ij} a generic calibration coefficient, constituting the calibration matrix, that is used to take into account the cross-talk effect. Since load cells' primary transducers work in their linear field, the calibration coefficients can be considered constant in the measurement range of the load cells.

Calibration coefficients have been obtained by positioning a graduate flat surface on the chair LP (Figure 4). The graduate surface has specific reference points that allow the application of controlled loads on the chair LP; as an example, by using known loads it is possible to apply only the F_z component or specific M_x and M_y, since the equidistant orthogonal axes from load cells couples are identified. Thus, considering three different load conditions, and reading the correspondent voltage output, it is possible to apply three times Equations (9) to obtain the calibration coefficients.

Figure 4. Load cells calibration setup performed using a graduate reference surface positioned on the chair LP and known loads.

2.2. Experimental Protocol

An experimental campaign has been designed and performed to extract the UCOP coordinates while asking the volunteers seated on the chair to undergo a task sequence with increasing levels of cognitive engagement defined through a dedicated test (i.e., Stroop test).

The Stroop test has been successfully employed for driving volunteers from a natural and relaxed position on the seat of a chair to different ones associated with a stressing condition while increasing the difficulty level of the performed task. Details of the designed Stroop test are given in the following.

2.2.1. Stroop Test

In the Strop test, a stress condition in the participants is induced, by asking them to perform a series of similar cognitive tasks with an increasing level of difficulty and engagement [37]. In previous works, it has been demonstrated that the increasing engagement in such kinds of tests gives rise to a different level of stress in the participant [38] and as a consequence, a different sitting posture on the chair is taken [21].

The test used in this study is based on displaying some words on a screen that the participant has to read in a predefined period of time: in particular, the selected words are the name of a color (e.g., “blue”, “red”, “black”, etc.) and have been displayed written in black and white in a first phase while in a colored form in a second phase of the test. To best achieve a variation of the cognitive engagement and to increase the level of stress induced in the task, the phases are planned in order to induce the Stroop effect: in the first phase of the test, the participant is instructed through written indications to read the words displayed on the screen, while in the second phase he/she is invited to read aloud the color of the word, regardless of the meaning of the word (this will be called PHA in the following). Then the combinations (color–meaning) in the successive phases are: the name and the color are matching (e.g., the word “blue” is displayed using a blue color, PHB in the following); and the name and the color are not matching (e.g., the word “blue” is displayed using a red color, PHC in the following). Different sets of words are displayed in sequence, giving a fixed time slot to the participant to complete the reading of each set. In PHB, the task is very easy since the color of the word corresponds to its meaning. In PHC, the task is more demanding, and the number of mistakes

made by the participant increases (e.g., not all words in the set are read or the meaning of the word is read instead of its color). This is mainly due to the time provided to the participants to complete the task being limited. Moreover, the participant is warned of the errors he/she made, and this induces a stressing condition that usually is maintained and growing till the end of the test.

In this work, a Stroop test consisting of 25 PowerPoint slides was realized and it was presented to a population of volunteers while sitting on the designed chair. In particular, according to the results obtained in [21], the test sequence (PHA, PHB, PHC) is described in the following and shown in Figure 5:

(a) PHA: 6 sets of black and white words representing color names, that were included in the test to make the participant familiar with the required task (i.e., the readings of words on a display in a predefined time slot) (Figure 5a).
(b) PHB: 6 sets of colored words representing color names with a correspondence between the adopted color and the meaning (Figure 5b).
(c) PHC: 12 sets of colored words representing color names with mismatching color and meaning (Figure 5c).

Figure 5. Black and white color words (**a**); matching color words (**b**); and non-matching color words (**c**) displayed respectively during phases PHA, PHB and PHC of the Stroop test.

Within each phase, the word set presented to the volunteers has an increasing number of words composing a slide that has been displayed in full screen mode. A fixed time delay for transition between consecutive sets has been set according to [21] to be able to induce the Stroop effect. Moreover, this choice allows for uniform test conditions for the whole population of participants, together with the standardization of the adopted font size (96 pt.) for all the displayed words.

The adopted settings are reported in Table 1.

Table 1. Schedule of the Stroop test—in the first phase the words are in black and white, in the second phase the color of words matches the word meaning, and in the third phase the color of words does not match the word meaning.

	Number of Words Per Set	Number of Slides	Time Per Slide [s]
PHA: Black and white words	3	2	2
	4	2	2.5
	5	1	3
	6	1	3.5
PHB: Colored words with color matching the meaning	3	2	2
	4	2	2.5
	5	1	3
	6	1	3.5
PHC: Colored words with color not matching the meaning	3	2	2.5
	4	2	3
	5	2	3.5
	6	2	4
	9	2	6
	12	2	8

2.2.2. Experimental Protocol

The tests have been presented to a group of 95 participants (61 males and 34 females), with age of 29 ± 12 years (mean ± SD). All participants filled a form declaring their agreement to participate in this scientific test. All volunteers had no visual impairments (i.e., none of them wore glasses or contact lenses, all volunteers were checked for color blindness) and in general, were healthy with no apparent or declared mobility problems (e.g., use of walking aids). Since the sets of words were written in Italian, all the selected participants were native Italian speakers. The participants were recruited among the population visiting the "Maker Faire 2019" (The European edition, Rome, Italy).

Since the chair was equipped only with force sensors on the seat, the backrest was removed, so the chair was used like a stool in its use during the test. Each participant was invited to sit in a natural position, without crossing their legs. Participants were not informed about the scope of the test before conducting it, in order not to influence their behavior during its execution. Participants were briefly instructed about the tasks to be conducted, and further detailed instructions (i.e., "read the word on the slide" or "read the color of the words") were provided during the displaying of the words sets (i.e., at the beginning and at each phase transition of the test). The participants were asked to read aloud as quick as possible the words' meaning for the sets displayed in PHA and PHB, and the color of each word regardless of its meaning for the sets displayed in PHC. After the conclusion of the test, each participant was informed about the presence of the sensors under the seat and about the recorded data. Moreover, participants were informed that they were part of a scientific study, and everybody confirmed the given consensus to be part of the studied population. Nobody felt the presence of sensors during the test or a feeling different than that of sitting on a normal stool. Recorded data were stored in a database, together with the personal information of the volunteers (i.e., age and gender), and associated to a code for each participant. A list matching the participant name and the code was encrypted and stored in a different storage device from that of the database.

2.3. Data Analysis

From the acquired and calibrated dynamic data (i.e., F_z, M_x and M_y), the UCOP coordinates, X_{UCOP} and $Y_{UCOP,}$ with respect to the chair origin were calculated for each phase according to Equation (1), removed of their average value for each phase, and low-pass filtered through a third-order zero phase Butterworth digital filter with a 20-Hz cut-off frequency. This produced, for each phase, a 2D time series, {X_{UCOP}A,Y_{UCOP}A}, {X_{UCOP}B,Y_{UCOP}B} and {X_{UCOP}C,Y_{UCOP}C}, respectively. Then, the corresponding resulting distances RDA, RDB and RDC (i.e., the magnitude of the displacement of the instantaneous position of UCOP from its mean value) were calculated. From these time series, in agreement with the definitions given in [22], mean distance values (MD, MDX and MDY), RMS distance values (RDIST, RDISTX and RDISTY), range values (RANGE, RANGEX and RANGEY), Mean Velocity values (MVELO, MVELOX and MVELOY), the 95% confidence circle area value (AREA-CC), the 95% confidence ellipse area value (AREA-CE) and the sway area value (SWAREA) were calculated for every subject and for each phase. Moreover, for each parameter and for each phase, the mean value and the standard deviation were calculated for all subjects. Pairwise t-tests were conducted with phases as a grouping factor for all the calculated parameters. In order to verify whether there was a significant difference in parameters among the three phases, a p-value < 0.05 was chosen, but also different acceptable values of p (i.e., $p < 0.01$, $p < 0.001$ and $p < 0.0001$) were selected to indicate different levels of statistical effect.

3. Results

The time trends of X_{UCOP}, Y_{UCOP} and RD for one of the participants are displayed in Figure 6, together with the plots of the corresponding stabilograms (i.e., X_{UCOP}-vs-Y_{UCOP} plot). Different colors are used in the figures to highlight differences among the three phases (green for PHA, red for PHB, and black for PHC).

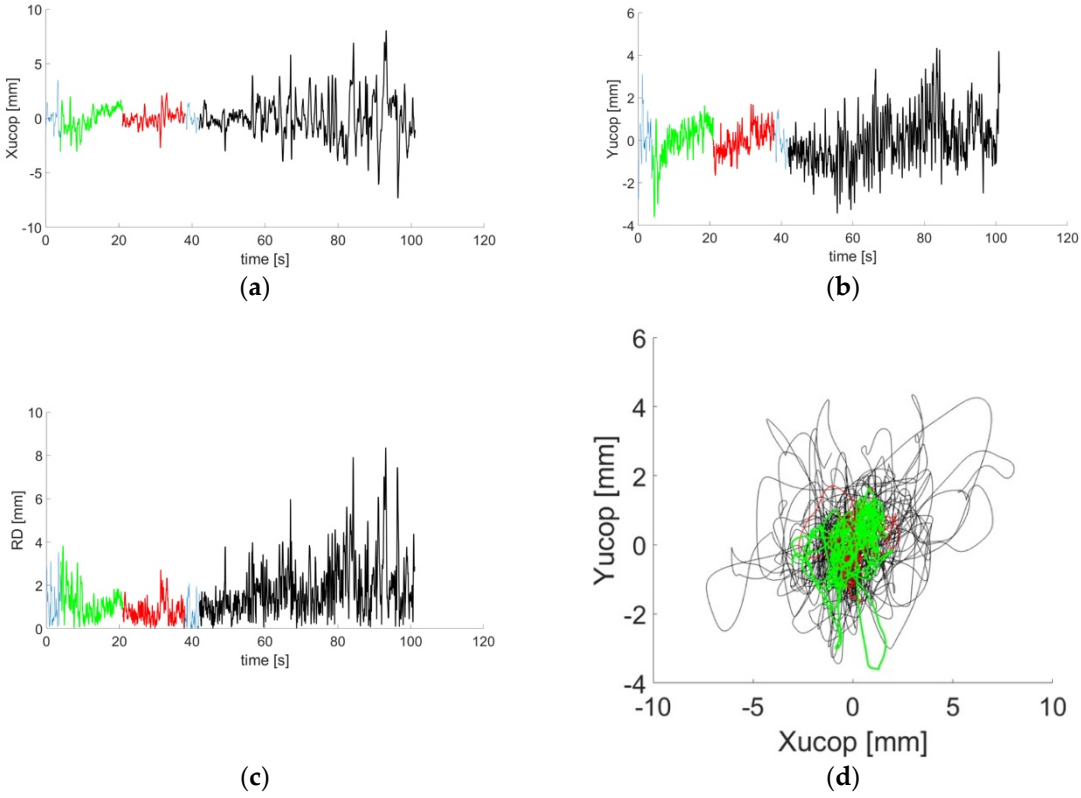

Figure 6. Time trends of the XUCOP (**a**), YUCOP (**b**) and RD (**c**), together with the corresponding stabilogram (**d**) for one of the participants.

In the displayed time series, the increase of the X_{UCOP} and Y_{UCOP} range, together with the calculated RD, is remarkable throughout the test from the least engaging part (PHA) to the most demanding one (PHC). In addition, the stabilogram plot shows a significant increase in the swept area in PHC as compared to PHA and PHB. This increment of the seated sway excursion demonstrates that when volunteers are involved in a demanding cognitive task, there is a lower stability on the seat with respect to the phases of the test where the task to be performed is simpler. This can be due to the growing of a stressing condition that can cause a different position on the chair, as demonstrated in [21], and can also induce a different dynamic behavior.

The results of the statistical analysis are shown in Table 2, together with the mean values of the calculated parameters for all participants, and the corresponding standard deviations. For all parameters, except the sway area, the difference between coupled distributions resulted highly significant for PHA vs. PHC and PHB vs. PHC, thus validating the hypothesis that a different strategy for controlling the sway is assumed by subjects when cognitive engagement increases. Moreover, for the range parameters (i.e., RANGE, RANGEX and RANGEY), the difference between PHA and PHB resulted significant: the difference is higher for the y coordinate (i.e., anteroposterior) and this can be explained by the biomechanics of the hip. During a seated position, this joint has reduced swinging along the mediolateral direction (i.e., x direction) with respect to the anteroposterior one (i.e., y direction), so when posture is not well controlled, a greater instability along y is found.

Table 2. UCOP-based descriptive parameters computed for all the volunteers: for each parameter the mean and std values calculated over all participants have been reported for each of the three phases of the test. For the same parameters, the p-value obtained from the multiple pairwise t-tests between phases have been calculated and different level of significance have been assessed as reported in the following: * $p < 0.05$, ** $p < 0.01$, **** $p < 0.0001$.

Measure	PHA		PHB		PHC		*p*-values					
	Mean	std	Mean	std	Mean	std	PHA-PHB	PHA-PHC	PHB-PHC	PHA-PHB	PHA-PHC	PHB-PHC
mean distance (mm)	**1.95**	**1.30**	**1.66**	**1.44**	**4.72**	**4.14**	**0.1481**	**1.06×10^{-15}**	**1.22×10^{-10}**		****	****
mean distance x (mm)	1.16	0.74	1.07	1.06	2.84	2.83	0.5376	2.90×10^{-12}	4.68×10^{-8}		****	****
mean distance y (mm)	1.30	1.05	1.03	0.93	3.14	2.85	0.0628	4.21×10^{-15}	9.41×10^{-11}		****	****
rms distance (mm)	**2.45**	**1.67**	**1.96**	**1.69**	**5.77**	**5.03**	**0.0457**	**6.38×10^{-16}**	**4.18×10^{-11}**	*	****	****
rms distance x (mm)	1.59	1.03	1.40	1.35	3.81	3.61	0.2878	2.50×10^{-13}	6.02×10^{-9}		****	****
rms distance y (mm)	1.77	1.44	1.30	1.10	4.14	3.74	0.0124	2.18×10^{-15}	2.66×10^{-11}	*	****	****
range (mm)	**13.11**	**9.57**	**9.70**	**7.93**	**37.54**	**33.40**	**0.0082**	**7.41×10^{-20}**	**2.25×10^{-13}**	**	****	****
range x (mm)	10.25	7.17	8.14	7.12	28.72	27.62	0.0435	9.16×10^{-17}	3.69×10^{-11}	*	****	****
range y (mm)	10.72	8.82	7.30	5.20	29.89	26.80	0.0014	9.68×10^{-20}	8.33×10^{-14}	**	****	****
mean velocity (mm/s)	**11.33**	**5.47**	**10.78**	**5.84**	**4.72**	**2.97**	**0.5044**	**3.98×10^{-20}**	**2.32×10^{-16}**		****	****
mean velocity x (mm/s)	6.86	3.31	6.44	3.72	2.79	1.84	0.4176	1.55×10^{-19}	3.48×10^{-15}		****	****
mean velocity y (mm/s)	7.48	3.92	7.22	4.30	3.18	2.07	0.6617	3.81×10^{-17}	2.80×10^{-14}		****	****
95% confidence circle area (mm^2)	**6.19**	**2.11**	**5.35**	**2.09**	**9.20**	**3.86**	**0.0067**	**4.54×10^{-19}**	**4.25×10^{-15}**	**	****	****
95% confidence ellipse area (mm^2)	**66.36**	**94.90**	**47.43**	**79.17**	**433.16**	**732.97**	**0.1371**	**1.70×10^{-10}**	**8.27E-07**		****	****
sway area (mm^2/s)	**10.36**	**13.32**	**7.45**	**10.19**	**11.75**	**18.59**	**0.0932**	**0.1145**	**0.0497**			*

Finally, significant differences can be observed in the RMS distance values (RDIST and RDISTY) and in the 95% confidence circle area (mm^2).

Figures 7–11 show the graphical representation of the calculated parameters' distributions. For MD values, it is noticeable that the increased engagement in PHC for the requested task significantly increases the distance from the UCOP center in both sway directions (Figure 7). The same results can be observed considering the RMS distances values (Figure 8). For both parameters, a greater excursion in the y direction (i.e., anteroposterior) is noticeable.

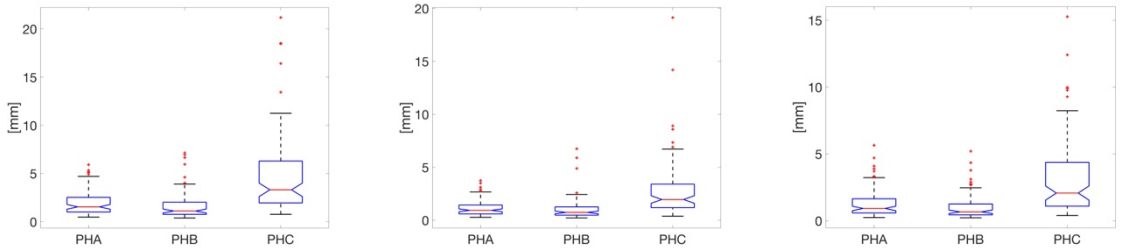

Figure 7. Mean distance distributions for each of the three phases PHA, PHB and PHC: (**a**) MD distributions, (**b**) MDX distributions and (**c**) MDY distributions.

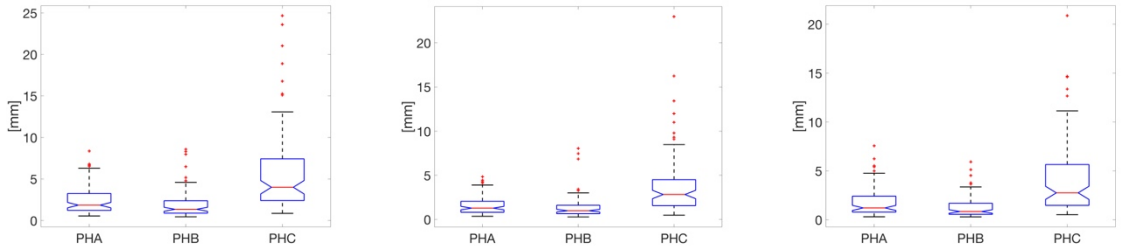

Figure 8. RMS distance distributions for each of the three phases PHA, PHB and PHC: (**a**) RDIST distributions, (**b**) RDISTX distributions and (**c**) RDISTY distributions.

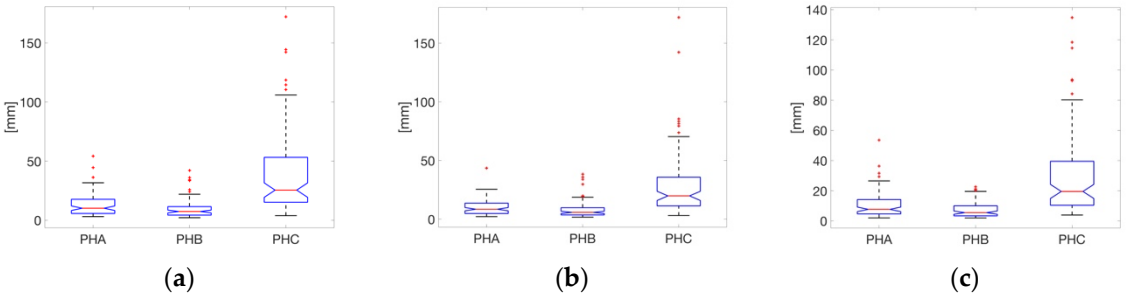

Figure 9. Range distributions for each of the three phases PHA, PHB and PHC: (**a**) RANGE distributions, (**b**) RANGEX distributions and (**c**) RANGEY distributions.

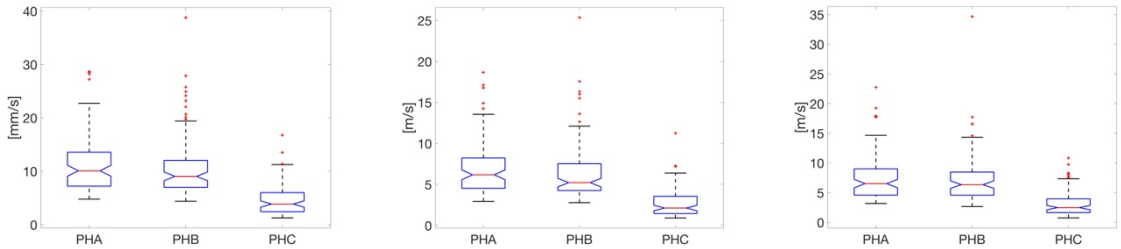

Figure 10. Mean velocity distributions for each of the three phases PHA, PHB and PHC: (**a**) MVELO distributions, (**b**) MVELOX distributions and (**c**) MVELOY distributions.

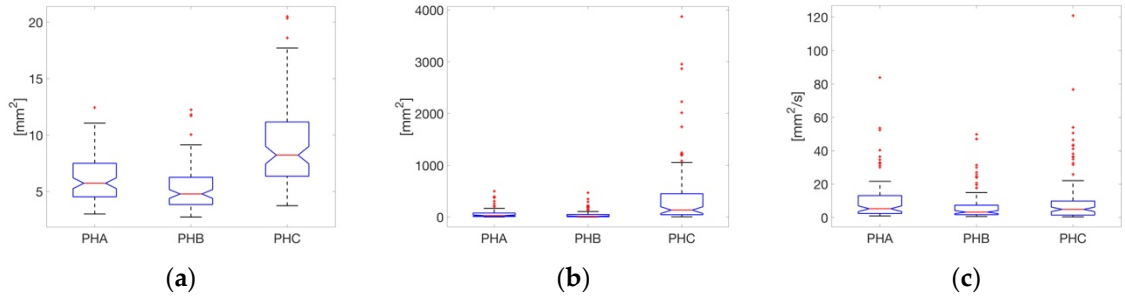

Figure 11. Area Parameters distributions for each of the three phases PHA, PHB and PHC: (**a**) AREA-CC distributions, (**b**) AREA-CE distributions and (**c**) SWAREA distributions.

These results are confirmed considering the range parameters distributions (Figure 9), where higher values of the maximum and minimum coordinates result in the UCOP excursion during PHC. It is also important to note that the range values in PHB are significantly lower than the ones in PHA: it can be speculated that after the first phase of the test, the volunteers reach a stable position where they feel comfortable both with the sitting posture and in performing the task. This condition is strongly modified in PHC and, since the total duration of the test is chosen not to induce muscular fatigue, the change of strategy in swaying can be explained by the increase in the difficulty of the task that induces a higher cognitive engagement.

Considering the velocity parameters distributions (Figure 10), a significant decrease in the velocity of the UCOP trajectory appeared in PHC, compared to both PHA and PHB. This evidence, together with the assessed high excursion, can confirm a decreased capability in controlling equilibrium in the most demanding condition: in fact, if the greater excursion would have been caused by an active rapid movement, the velocity would not have decreased as shown. The decrease of these values can therefore be explained by a reduced capability in controlling the UCOP trajectory and "corrective" actions performed to remain in a seated equilibrium.

Finally, area parameters distributions (Figure 11) reveal a larger area swept by the UCOP trajectory and a general instability achieved by subjects in PHC than in PHA and PHB, especially considering the 95% confidence circle and ellipse areas.

4. Conclusions

In this paper, a new system to assess if engaging cognitive activities influence the postural sway of a subject seated on a chair is presented. The designed and realized system, based on a chair equipped with force sensors that allows the dynamics description of the examined motor act, provides the time trend of the volunteers' position. These data can provide useful information on the adopted strategies in the seated postural control in subjects directed towards a complex cognitive task in a reduced amount of time. The obtained results show a significant difference in sway strategy and a coherent variation for a high number of examined volunteers, thus supporting the hypothesis that the higher demand the cognitive task has, the lower the stability in the seated posture. The realized system is

based on the integration of sensors on a normal office chair, whose physical features are not modified. Moreover, the system is designed to be powered with batteries and can be improved by embedding a wireless transmission. All these features allow the use of the chair in a wide range of situations, such as a smart working environment, where the device can provide useful information about the risk related to working activities due to the task-induced cognitive load.

As a future development, the system could be further validated by using additional techniques for cognitive load assessment, such as EEG analysis, testing the same setup in conditions similar to the ones presented in this work.

The realized device will be completed with seat backrest sensing, in order to obtain a system that allows a complete analysis of the adopted posture. This can be very useful to monitor activities that require a prolonged seated time, and where the cognitive engagement is constant: in this case, the postural sway could be a useful indicator of global fatigue, thus giving important information on the correct time schedule of the performed working tasks and to prevent all the pathologies related to the adoption of improper seated postures.

Author Contributions: Conceptualization, D.B. and F.B.; methodology, D.B., S.C., and F.B.; software, D.B. and F.B.; validation, D.B., and S.C.; formal analysis, D.B. and F.B.; investigation D.B., M.S., and F.B.; resources, S.C. and M.S.; writing—original draft preparation, D.B. and F.B.; writing—review and editing, D.B., S.C., M.S. and F.B. All authors have read and agreed to the published version of the manuscript.

Funding: This research received no external funding.

Acknowledgments: The authors would like to thank Moses Mariajoseph, Giorgio Scordino and Arturo Zezza for their contribution in recruiting the volunteers for the experimental campaign.

Conflicts of Interest: The authors declare no conflict of interest.

References

1. Mielke, G.I.; Burton, N.W.; Turrellc, G.; Browna, W.J. Temporal trends in sitting time by domain in a cohort of mid-age Australian men and women. *Maturitas* **2018**, *116*, 108–115. [CrossRef]
2. Medina, C.; Tolentino-Mayo, L.; López-Ridaura, R.; Barquera, S. Evidence of Increasing Sedentarism in Mexico City during the Last Decade: Sitting Time Prevalence, Trends, and Associations with Obesity and Diabetes. *PLoS ONE* **2017**, *12*, e0188518. [CrossRef] [PubMed]
3. Owen, N.; Sparling, P.B.; Healy, G.N.; Dunstan, D.W.; Matthews, C.E. Sedentary Behavior: Emerging Evidence for a New Health Risk. *Mayo Clin. Proc.* **2010**, *85*, 1138–1141. [CrossRef] [PubMed]
4. Loyen, A.; Chey, T.; Engelen, L.; Bauman, A.; Lakerveld, J.; van der Ploeg, H.P.; Brug, J.; Chau, J.Y. Recent Trends in Population Levels and Correlates of Occupational and Leisure Sitting Time in Full-Time Employed Australian Adults. *PLoS ONE* **2018**, *13*, e0195177. [CrossRef] [PubMed]
5. Ekelund, U.; Steene-Johannessen, J.; Brown, W.J.; Fagerland, M.W.; Owen, N.; Powell, K.E.; Bauman, A.; Lee, I.M. Lancet Physical Activity Series 2 Executive Committe; Lancet Sedentary Behaviour Working Group. Does physical activity attenuate, or even eliminate, the detrimental association of sitting time with mortality? A harmonised meta-analysis of data from more than 1 million men and women. *Lancet* **2016**, *388*, 1302–1310. [CrossRef]
6. Ikegami, K.; Hirata, H.; Ishihara, H.; Guo, S. Development of a Chair Preventing Low Back Pain with Sitting Person Doing Hand Working at the Same Time. In Proceedings of the 2018 IEEE International Conference on Mechatronics and Automation (ICMA), Changchun, China, 5–8 August 2018; pp. 1760–1764. [CrossRef]
7. Kim, J.B.; Yoo, J.K.; Yu, S. Neck–Tongue Syndrome Precipitated by Prolonged Poor Sitting Posture. *Neurol. Sci.* **2014**, *35*, 121–122. [CrossRef]
8. Sardini, E.; Serpelloni, M.; Pasqui, V. Daylong sitting posture measurement with a new wearable system for at home body movement monitoring. In Proceedings of the 2015 IEEE International Instrumentation and Measurement Technology Conference (I2MTC), Pisa, Italy, 11–14 May 2015; pp. 652–657. [CrossRef]
9. Dunne, L.; Walsh, P.; Smyth, B.; Caulfield, B. Design and Evaluation of a Wearable Optical Sensor for Monitoring Seated Spinal Posture. In Proceedings of the 2006 10th IEEE International Symposium on Wearable Computers, Montreux, Switzerland, 11–14 October 2006; pp. 65–68.

10. Fida, B.; Bernabucci, I.; Bibbo, D.; Conforto, S.; Proto, A.; Schmid, M. The Effect of Window Length on the Classification of Dynamic Activities through a Single Accelerometer, Biomedical Engineering. In Proceedings of the IASTED International Conference Biomedical Engineering (BioMed), Zurich, Switerzland, 23–25 June 2014.
11. Fida, B.; Bibbo, D.; Bernabucci, I.; Proto, A.; Conforto, S.; Schmid, M. Real Time Event-Based Segmentation to Classify Locomotion Activities through a Single Inertial Sensor. In Proceedings of the 5th EAI International Conference on Wireless Mobile Communication and Healthcare, London, UK, 14–16 October 2015.
12. Yamato, Y. Experiments of Posture Estimation on Vehicles Using Wearable Acceleration Sensors. In Proceedings of the 2017 IEEE 3rd International Conference on Big Data Security on Cloud (BigDataSecurity), IEEE International Conference on High Performance and Smart Computing, (HPSC) and IEEE International Conference on Intelligent Data and Security (IDS), Beijing, China, 26–28 May 2017; pp. 14–17.
13. Massé, F.; Bourke, A.K.; Chardonnens, J.; Paraschiv-Ionescu, A.; Aminian, K. Suitability of commercial barometric pressure sensors to distinguish sitting and standing activities for wearable monitoring. *Med. Eng. Phys.* **2014**, *36*, 739–744. [CrossRef]
14. Estrada, J.; Vea, L. Sitting posture recognition for computer users using smartphones and a web camera. In Proceedings of the TENCON 2017 - 2017 IEEE Region 10 Conference, Penang, Malaysia, 5–8 November 2017; pp. 1520–1525. [CrossRef]
15. Amine Elforaici, M.E.; Chaaraoui, I.; Bouachir, W.; Ouakrim, Y.; Mezghani, N. Posture Recognition Using an RGB-D Camera: Exploring 3D Body Modeling and Deep Learning Approaches. In Proceedings of the 2018 IEEE Life Sciences Conference (LSC), Montreal, QC, Canada, 28–30 October 2018; pp. 69–72.
16. Wang, W.-J.; Chang, J.-W.; Haung, S.-F.; Wang, R.-J. Human Posture Recognition Based on Images Captured by the Kinect Sensor. *Int. J. Adv. Robot. Syst.* **2016**, *13*. [CrossRef]
17. D'Anna, C.; Varrecchia, T.; Bibbo, D.; Orsini, F.; Schmid, M.; Conforto, S. Effect of different smartphone uses on posture while seating and standing. In Proceedings of the 2018 IEEE International Symposium on Medical Measurements and Applications (MeMeA), Rome, Italy, 11–13 June 2018.
18. Ishac, K.; Suzuki, K. LifeChair: A Conductive Fabric Sensor-Based Smart Cushion for Actively Shaping Sitting Posture. *Sensors* **2018**, *18*, 2261. [CrossRef]
19. Zemp, R.; Tanadini, M.; Plüss, S.; Schnüriger, K.; Singh, N.B.; Taylor, W.R.; Lorenzetti, S. Application of Machine Learning Approaches for Classifying Sitting Posture Based on Force and Acceleration Sensors. *BioMed Res. Int.* **2016**, *2016*, 5978489. [CrossRef]
20. Roh, J.; Park, H.J.; Lee, K.J.; Hyeong, J.; Kim, S.; Lee, B. Sitting Posture Monitoring System Based on a Low-Cost Load Cell Using Machine Learning. *Sensors* **2018**, *18*, 208. [CrossRef] [PubMed]
21. Bibbo, D.; Carli, M.; Conforto, S.; Federica, B. A Sitting Posture Monitoring Instrument to Assess Different Levels of Cognitive Engagement. *Sensors* **2019**, *19*, 455. [CrossRef] [PubMed]
22. Prieto, T.E.; Myklebust, J.; Hoffmann, R.; Lovett, E.; Myklebust, B. Measures of postural steadiness: Differences between healthy young and elderly adults. *IEEE Trans. Biomed. Eng.* **1996**, *43*, 956–966. [CrossRef] [PubMed]
23. Błaszczyk, J.W. The use of force-plate posturography in the assessment of postural instability. *Gait Posture* **2016**, *44*, 1–6. [CrossRef] [PubMed]
24. Morasso, P.G.; Sanguineti, V. Ankle Muscle Stiffness Alone Cannot Stabilize Balance during Quiet Standing. *J. Neurophysiol.* **2002**, *88*, 2157–2162. [CrossRef] [PubMed]
25. Schmid, M.; Conforto, S.; Bibbo, D.; D'Alessio, T. Respiration and postural sway: Detection of phase synchronizations and interactions. *Hum. Mov. Sci.* **2004**, *23*, 105–119. [CrossRef]
26. Conforto, S.; Schmid, M.; Camomilla, V.; D'Alessio, T.; Cappozzo, A. Hemodynamics as a possible internal mechanical disturbance to balance. *Gait Posture* **2001**, *14*, 28–35. [CrossRef]
27. Goodworth, A.D.; Tetreault, K.; Lanman, J.; Klidonas, T.; Kim, S.; Saavedra, S. Sensorimotor control of the trunk in sitting sway referencing. *J. Neurophysiol.* **2018**, *120*, 37–52. [CrossRef]
28. Galin, D.; Johnstone, J.; Herron, J. Effects of task difficulty on EEG measures of cerebral engagement. *Neuropsychologia* **1978**, *16*, 461–472. [CrossRef]
29. Hou, X.; Liu, Y.; Sourina, O.; Tan, Y.R.E.; Wang, L.; Mueller-Wittig, W. EEG Based Stress Monitoring. In Proceedings of the 2015 IEEE International Conference on Systems, Man, and Cybernetics, Kowloon, China, 9–12 October 2015; pp. 3110–3115. [CrossRef]

30. Russ, S.; MacKenzie, R.K.; Morrison, I.; Morse, J.; Johnston, M.; Bell, C.; Patey, R. 0094 The impact of demand and cognitive load on stress and performance in 2nd year medical students: A simulation study. *BMJ Simul. Technol. Enhanc. Learn.* **2015**, *1*, A10. [CrossRef]
31. West, R.; Bell, M.A. Stroop color—word interference and electroencephalogram activation: Evidence for age-related decline of the anterior attention system. *Neuropsychology* **1997**, *11*, 421–427. [CrossRef] [PubMed]
32. Bonnet, C.T.; Davin, D.; Hoang, J.-Y.; Baudry, S. Relations between Eye Movement, Postural Sway and Cognitive Involvement in Unprecise and Precise Visual Tasks. *Neuroscience* **2018**, *416*, 177–189. [CrossRef] [PubMed]
33. Stins, J.F.; Michielsen, M.E.; Roerdink, M.; Beek, P.J. Sway regularity reflects attentional involvement in postural control: Effects of expertise, vision and cognition. *Gait Posture* **2009**, *30*, 106–109. [CrossRef] [PubMed]
34. Leach, J.M.; Mancini, M.; Kaye, J.A.; Haye, T.L.; Horak, F.B. Day-to-Day Variability of Postural Sway and Its Association With Cognitive Function in Older Adults: A Pilot Study. *Front. Aging Neurosci.* **2018**, *10*, 126. [CrossRef]
35. Bibbo, D.; Gabriele, S.; Scorza, A.; Schmid, M.; Sciuto, S.A.; Conforto, S. Strain gauges position optimization in designing custom load cells for sport gesture analysis. In Proceedings of the IEEE 20th International Conference on E-Health Networking, Applications and Services (Healthcom), Ostrava, Czech Republic, 17–20 September 2018; pp. 1–6.
36. Bibbo, D.; Gabriele, S.; Scorza, A.; Schmid, M.; Sciuto, S.A.; Conforto, S. A Novel Technique to Design and Optimize Performances of Custom Load Cells for Sport Gesture Analysis. *IRBM* **2019**, *40*, 201–210. [CrossRef]
37. Stroop, J.R. Studies of interference in serial verbal reactions. *J. Exp. Psychol.* **1935**, *18*, 643–662. [CrossRef]
38. Renaud, P.; Blondin, J.-P. The Stress of Stroop Performance: Physiological and Emotional Responses to Color–Word Interference, Task Pacing, and Pacing Speed. *Int. J. Psychophysiol.* **1997**, *27*, 87–97. [CrossRef]